WATER RESOURCES RESEARCH, VOL. 49, 1–14, doi:10.1002/wrcr.20434, 2013

How does rapidly changing discharge during storm events affect transient storage and channel water balance in a headwater mountain stream?

Adam S. Ward,[1] Michael N. Gooseff,[2] Thomas J. Voltz,[3] Michael Fitzgerald,[4] Kamini Singha,[5] and Jay P. Zarnetske[6]

Received 24 October 2012; revised 6 July 2013; accepted 17 July 2013.

[1] Measurements of transient storage in coupled surface-water and groundwater systems are widely made during base flow periods and rarely made during storm flow periods. We completed 24 sets of slug injections in three contiguous study reaches during a 1.25 year return interval storm event (discharge ranging from 21.5 to 434 L s^{-1}) in a net gaining headwater stream within a steep, constrained valley. Repeated studies over a 9 day period characterize transient storage and channel water from prestorm conditions through storm discharge recession. Although the valley floor was always gaining from the hillslopes based on hydraulic gradients, we observed exchange of water from the stream to the valley floor throughout the study and flow conditions. Interpretations of transient storage and channel water balance are complicated by dynamic in-stream and near-stream processes. Metrics of transient storage and channel water balance were significantly different (95% confidence level) between the three study reaches and could be identified independently of stream discharge via analysis of normalized breakthrough curves. These differences suggest that the morphology of each study reach was the primary control on solute tracer transport. Unlike discharge, metrics of transient storage and channel water balance did not return to the prestorm values. We conclude that discharge alone is a poor predictor of tracer transport in stream networks during storm events. Finally, we propose a perceptual model for our study site that links hydrologic dynamics in 3-D along the hillslope-riparian-hyporheic-stream continuum, including down-valley subsurface transport.

Citation: Ward, A. S., M. N. Gooseff, T. J. Voltz, M. Fitzgerald, K. Singha, and J. P. Zarnetske (2013), How does rapidly changing discharge during storm events affect transient storage and channel water balance in a headwater mountain stream?, *Water Resour. Res.*, *49*, doi:10.1002/wrcr.20434.

1. Introduction and Background

[2] The bidirectional interaction of streams and their aquifers is ecologically important [e.g., *Brunke and Gonser*, 1997; *Krause et al*., 2011; *Boulton et al*., 1998]. The ecological function of the hyporheic zone has been primarily quantified during stable base flow conditions; however, the role of these exchanges in biogeochemical processes is likely altered by hydrological dynamics during storm events [e.g., *Gu et al*., 2008; *Zarnetske et al*., 2012]. Unfortunately, little is known about how headwater mountain streams and their riparian and hyporheic zones exchange water, mass, and energy during storm events. Current conceptual models lack information about responses across the stream-hyporheic-riparian-hillslope continuum during storm events, and lack information about internal dynamics and processes during storm events. Our understanding of the exchange of stream water between surface streams and their hyporheic and riparian zones during storm events is based primarily on simple conceptual models or idealized numerical models [e.g., *Wondzell and Swanson*, 1996; *Shibata et al*., 2004], with only one study reporting dilution of a constant-rate tracer during a storm event [*Triska et al*., 1990]. To the best of our knowledge, repeated solute tracer studies during storm events to quantify the dynamics of transient storage and channel water balance (i.e., stream water exchange) during these hydrologically dynamic periods have not been reported. The

Additional supporting information may be found in the online version of this article.

[1]Department of Earth and Environmental Sciences, University of Iowa, Iowa City, Iowa, USA.
[2]Department of Civil and Environmental Engineering, Colorado State University, Fort Collins, Colorado, USA.
[3]Faculty of Civil Engineering and Architecture, Division of Water Sciences, University of Applied Sciences Dresden, Dresden, Germany.
[4]National Ecological Observatory Network, Boulder, Colorado, USA.
[5]Hydrologic Science and Engineering Program, Colorado School of Mines, Golden, Colorado, USA.
[6]Department of Geological Sciences, Michigan State University, East Lansing, Michigan, USA.

Corresponding author: A. S. Ward, Department of Earth and Environmental Sciences, University of Iowa, 36 Trowbridge Hall, Iowa City, IA 52242, USA. (adam-ward@uiowa.edu)

0043-1397/13/10.1002/wrcr.20434

objective of this study is to quantify changes in transient storage and channel water balance during storm events. Specifically, we will address two questions (1) How do metrics of transient storage and channel water balance vary in response to stream discharge changes during storm events?, and (2) Are solute tracer signals modified by stream reaches in a predictable pattern, independent of discharge? The term "modify" in this study is used to describe the change in the observed solute tracer time series between two observation points on the stream and across the different storm flow conditions.

[3] A growing body of work considers simultaneous, bidirectional exchange between the catchment and the stream during base flow conditions [e.g., *Payn et al*., 2009; *Jencso et al*., 2010; *Covino et al*., 2011; *Ward et al*., 2013b]. These studies primarily employ solute tracer and water balance approaches. They show that the catchment form is one primary control on exchange of stream water and solutes with the near-stream subsurface. Geologic heterogeneities and catchment structure both control fluxes in the riparian zone, commonly represented as fluxes lateral to the streambed or along hyporheic flow paths [e.g., *Jencso and McGlynn*, 2011; *Ward et al*., 2012; *Payn et al*., 2012]. At larger scales (e.g., alluvial valleys and/or floodplains), these exchanges are commonly conceptualized to include a down-valley subsurface flow that may have longer transit times [e.g., *Woessner*, 2002; *Poole*, 2002; *Stanford and Ward*, 1993; *Larkin and Sharp*, 1992]. Still, solute tracer persistence in smaller valley bottoms has been observed and attributed to the bedrock confinement of valley bottom deposits and steep down-valley topographic gradients [*Ward et al*., 2013b; *Voltz et al*., 2013].

[4] The description of streams at reach and larger scales as either net gaining or losing is a function of hydraulic gradients between streams and their aquifers. Within steep valley bottom environments, exchanges of water among the stream, hyporheic zone, and riparian zone persist across a wide range of hydrological conditions [e.g., *Ward et al*., 2012; *Voltz et al*., 2013; *Wondzell*, 2006; *Wondzell et al*., 2010]. From the perspective of hillslope hydrology, hysteretic responses have been reported linking hillslope discharge and stream discharge [*McGuire and McDonnell*, 2010]. From the perspective of the stream, movement of water into the near-stream subsurface is widely studied as both hyporheic exchange and bank storage across a range of net gaining and losing conditions [*Cardenas*, 2009; *Francis et al*., 2010; *Nowinski et al*., 2012]. A recent study by *Voltz et al*. [2013] demonstrates that although valley bottoms may consistently gain water from their hillslopes, substantial variability in hydraulic gradients near the channel and within the stream-hyporheic-riparian zone continuum persists during storm events. Their study further demonstrates that steep, confined systems are dominated by down-valley flow in the subsurface even during net gaining conditions. Down-valley flow in the subsurface can be an important aspect of hyporheic transport in some systems [*Kennedy et al*., 1984; *Jackman et al*., 1984; *Castro and Hornberger*, 1991; *Runkel et al*., 1998]. Finally, many models assume that the temporal response of the stream and riparian zone are synchronized at a given location. However, work by *Wondzell et al*. [2007, 2010] demonstrates that the stream integrates a range of temporal signals based on analysis of diel fluctuations in base flow discharge and that riparian-hyporheic-stream zones may not provide synchronized hydrologic and solute transport signals. Indeed, these temporal lags may give rise to the observed hysteresis between hillslope discharges and in-stream discharge [e.g., *McGuire and McDonnell*, 2010].

[5] Solute tracer studies are commonly applied to quantify interactions between streams and their valley bottoms. *Ward et al*. [2013b] present a conceptual framework of stream solute transport that partitions short-term and long-term storage to more completely characterize solute transport in the stream and the adjacent valley bottom. They showed that the boundary between short-term and long-term storage is the maximum temporal scale of tracer recovery, commonly called the "window of detection" in stream tracer studies [*Harvey and Bencala*, 1993; *Wagner and Harvey*, 1997; *Harvey and Wagner*, 2000]. Short-term storage describes tracer mass that is delayed from advective transport in the channel, but returns within the window of detection for a given tracer study (commonly referred to as "transient storage"). Long-term storage, on the other hand, describes tracer movement along the suite of flow paths that do not return to the downstream end of a stream reach within the window of detection for a given tracer study (commonly referred to as "channel water balance" or "gross gains and losses").

[6] Although both short- and long-term storage are studied through space under base flow conditions [*Payn et al*., 2009; *Covino et al*., 2011; *Ward et al*., 2013b], little is known about their dynamics in response to storm events. Therefore, we completed a series of stream solute tracer studies in three contiguous 50 m segments to quantify short- and long-term storage before, during, and after a large storm event. Twenty-four solute tracer injections were completed at each of the four study locations (i.e., bounding the upstream and downstream ends of the three contiguous study reaches) during a 9 day storm event and recession period. This study quantifies and relates metrics of stream water exchange with the near-stream subsurface (short- and long-term storage) to stream discharge and riparian water table conditions during a storm event. Further, this study considers the role of the tracer study's window of detection in interpretations of stream water exchange with the hyporheic and riparian zones.

2. Methods

2.1. Site Description

[7] This study was completed in Watershed 1 (WS1) at the H. J. Andrews Experimental Forest, located in the western Cascade Mountains of Oregon, United States (48°10'N, 122°15'W; Figure 1). The catchment has a steep valley gradient of 11.9% across three study reaches established for this study and the adjacent valley width is narrow (<20m). More specifically, Figure 1b shows the average slope of each study reach was 11.5% for the upstream reach, 16.6% for the middle reach, and 10.1% for the downstream reach. The morphology of each reach includes a series of pools, riffles, and steps. Each study reach was approximately 50 m in length along the valley axis, with the downstream-most point located approximately 2 m upstream of the WS1 stream gauge (Figure 1b). Many

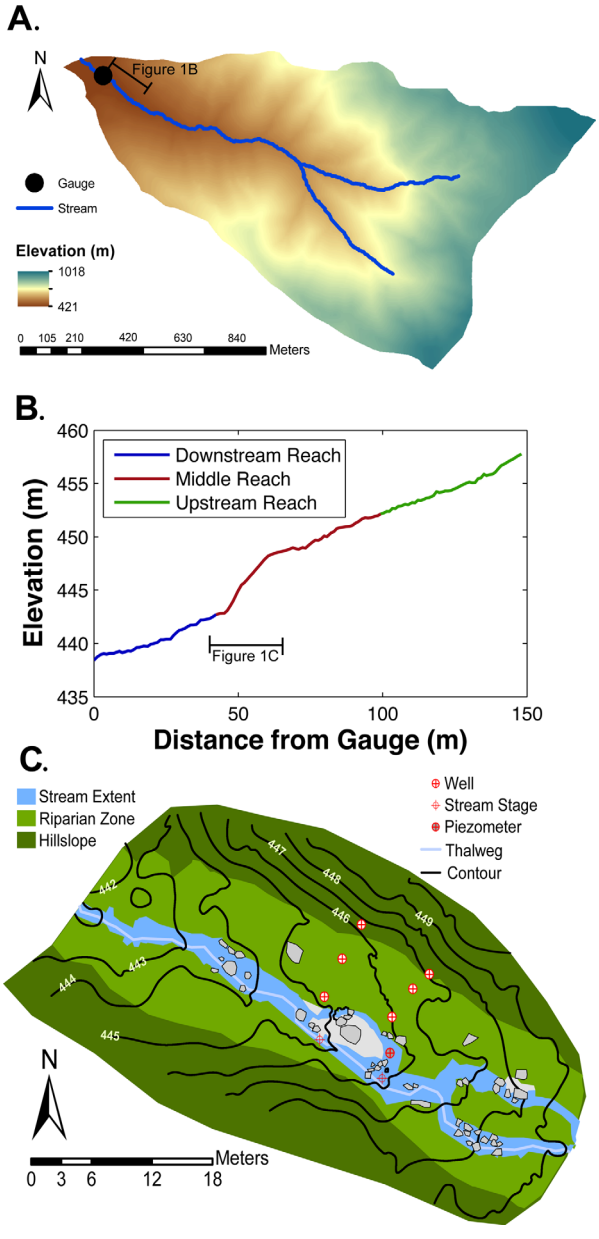

Figure 1. (a) Topography for the study catchment. (b) Profile along the stream centerline for our three study reaches, and (c) Plan view of the monitoring network in the middle study reach where water table elevations were observed.

geomorphic features, including sediment wedges that promote large head gradients and hyporheic exchange flows [*Kasahara and Wondzell*, 2003] were formed by boulders or large, fallen trees. The catchment ranges in elevation from 421 to 1018 m above mean sea level and has steep hillslopes (>50%) above geologically young bedrock [*Swanson and James*, 1975]. Valley bottom soils are shallow (1–2 m depth) loams [*Dyrness*, 1969] and have a documented saturated hydraulic conductivity of 1.7×10^{-5} m s^{-1} [*Wondzell et al.*, 2009]. At its outlet, the catchment drains 95.8 ha and discharge is gauged using a permanent flume maintained by the U.S. Forest Service. Precipitation records are from the Primary Meteorological Station at the H. J. Andrews Experimental Forest, which is approximately 0.5 km from the catchment outlet. The climate at the study site is characterized by wet, mild winters, and dry, cool summers. Storm events dominate the spring season, followed by generally dry summers, and prolonged base flow recession. This study took place during the last major storm event before the 2011 base flow recession period, consisting of precipitation patterns that resulted in two storm peaks with a minor recession between them (Figure 2). At the time of the study, the watershed was in recession from the annual peak flow due to seasonal snowmelt runoff.

[8] Watershed 1 contains a network of 32 shallow, small-diameter monitoring wells and piezometers installed in 1997. Wells outside of the stream channel during base flow were screened over their entire length. In-stream piezometers were screened over their bottom 5 cm, with screened sections located between 20 and 40 cm below the streambed. Further details of the well construction and installation are summarized by *Wondzell* [2006], and data collection details in these wells can be found in *Voltz et al.* [2013]. A subset of the network was instrumented with pressure transducers to monitor the potentiometric surface at 30 min intervals during the study period. Additionally, in-stream pressure transducers recorded the surface-water elevation at the intersection of well transects (oriented perpendicular to the stream) with the stream channel (Figure 1c). Water-level observations from monitoring wells, piezometers, and in-stream loggers were used to construct plots of hydraulic head and stream stage at two transects perpendicular to the valley located approximately 5 m from one another (Figure 1c). Potentiometric surfaces were plotted from piezometer and monitoring well data (Figure 3).

2.2. Solute Tracer Studies

[9] Twenty-four conservative tracer slug injections were completed at each of four locations (Figure 1b) during a 9 day period (1–9 June 2011). These injections resulted in 72 different tracer break through curves (i.e., documented tracer concentration time series across the three study reach locations). Sodium chloride (NaCl) was used as the conservative tracer, with individual tracer slug mass ranging from 198 to 1007 g (averaging 593 g). These tracer slug masses were scaled to use higher masses during higher discharge conditions. Injections were located upstream of fluid specific conductivity loggers at a distance sufficient for vertical and transverse mixing of the tracer across the stream cross section. The distance was scaled to have longer mixing lengths during higher discharges [after *Payn et al.*, 2009], and injections were made where riffles would aid in lateral mixing. Visual approximation, an accepted practice in the field, was the chosen method in recognition that this length would vary with discharge [e.g., *Payn et al.*, 2009; *Ward et al.*, 2013b]. Although theoretical mixing lengths can be calculated, accurate discharge estimates can be made with dilution gauging over smaller mixing lengths than those predicted by such formulas [e.g., *Fischer et al.*, 1979; *Florkowski et al.*, 1969]. Furthermore, mixing distances may not be well predicted by functions of channel morphology [*Day*, 1977].

[10] Break through curves were logged using fluid specific electrical conductivity as a surrogate for concentration, with dataloggers (Campbell Scientific, Logan, Utah,

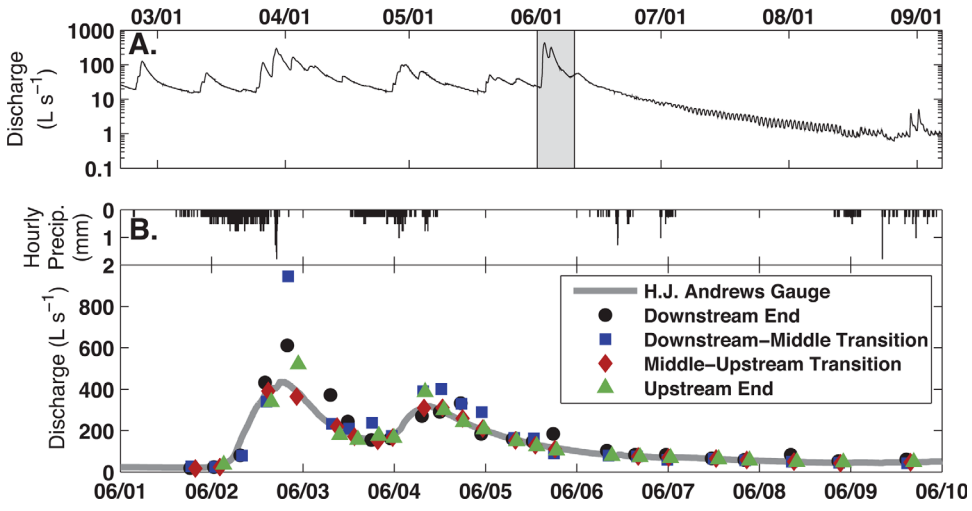

Figure 2. (a) Seasonal discharge from WS1 at the H. J. Andrews Experimental Forest. (b) Precipitation and discharge during the study period. Dilution gauging at four points bounded the upstream and downstream end of each study segment, with the downstream monitoring location immediately upstream of a permanently installed gauge station. Dates are MM/DD in 2010. The color scheme presented here is used for all subsequent figures in the manuscript.

USA) calibrated using a single curve based on known masses of tracer dissolved in stream water (as in, e.g., *Payn et al*. [2009]). No grab samples were collected during the study. Slug injections were chosen over constant rate injection methods to characterize the rapidly changing hydrologic conditions during the storm, and because they contain the same information as constant rate injections for conservative tracers [e.g., *Payn et al*., 2008; *Gooseff et al*.,

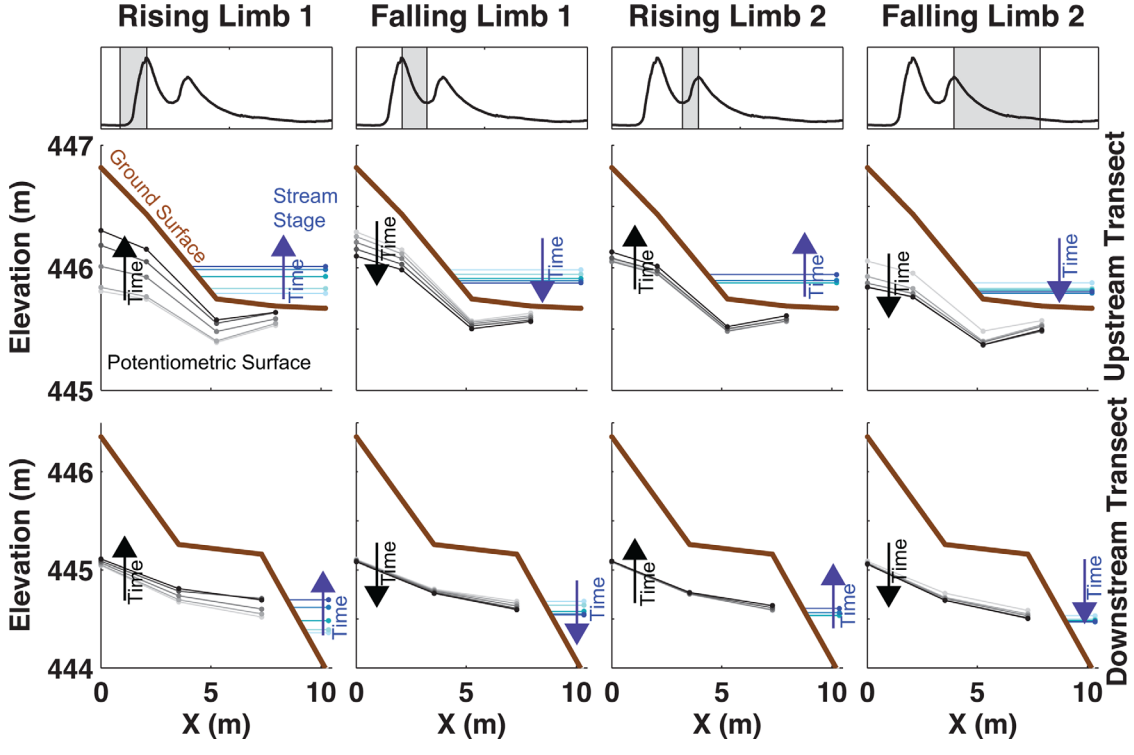

Figure 3. Water level observations are shown in the stream (blue lines extended horizontally from the observation point to the bank) and in monitoring wells and piezometers (black lines). Time segments depicted by each column are indicated by the shaded hydrograph at the top of each column. Darker colored lines represent conditions earlier in the time segment, and fade with equal temporal spacing to the end of the segment. Blue lines represent surface water elevations, and black lines potentiometric surface. Arrows indicate the direction of water level movement in each plot. The upstream and downstream segments are located on the north bank of the stream (left to right looking upstream; Figure 1c).

2008]. Prior to analysis, background fluid electrical conductivity was subtracted from the observed time series to isolate the change due to the tracer from pretracer conditions for each breakthrough curve. Background values for fluid electrical conductivity at the four injection locations were 38.2 ± 1.8, 38.4 ± 5.3, 38.6 ± 2.7, and 40.0 ± 5.0 μS/cm throughout the duration of the study (reported as mean ±1 standard deviation, downstream to upstream). It was not possible to replicate tracer releases during the storm event given the highly dynamic hydrologic conditions.

[11] Dilution gauging is subject to several sources of error [e.g., *Zellweger et al*., 1989]. In this study, high discharge observations at the downstream end of the middle study reach may have been affected by valley geomorphology. This location is at a large bedrock outcrop, where all down-valley subsurface flow resurfaces. Gauging at this location may have been more sensitive to underflow than other stations that were located on alluvial deposits. Finally, dilution gauging as applied in this study assumes steady state discharge during the time period between the tracer injection and the final observation of solute tracer at the monitoring point.

2.3. Long-Term Storage

[12] Solute tracer data collected in this study were analyzed using the channel water balance estimates described by *Payn et al*. [2009] to evaluate long-term storage conditions. Briefly, dilution gauging was used to calculate discharge at the downstream and upstream end of each study reach (Q_U and Q_D, respectively), and these discharges were used to calculate a net change in discharge for each reach, ($\Delta Q = Q_D - Q_U$). Tracer mass loss (M_{LOSS}) between the injection point and the downstream end of each study reach was used to quantify gross losses. Mass loss was calculated as

$$M_{LOSS} = M_{IN} - M_{REC} \quad (1)$$

where M_{IN} is the known tracer mass released into the stream and M_{REC} is the recovered tracer mass. The M_{REC} is calculated as

$$M_{REC} = Q_D \int_0^t C_{UD} dt \quad (2)$$

where C_{UD} is the background-corrected concentration time series for the upstream slug at the downstream monitoring location. *Payn et al*. [2009] define two end-members that bound the range of possible behaviors in the stream. The first assumes maximum dilution of the signal (i.e., all gains occur before all losses), while the second assumes maximum loss of tracer (i.e., all losses occur before all gains, defined as $Q_{LOSS,MIN}$ and $Q_{LOSS,MAX}$, respectively. $Q_{LOSS,MIN}$ and $Q_{LOSS,MAX}$ are calculated as

$$Q_{LOSS,MIN} = \frac{M_{LOSS}}{\int_0^t C_U(t) dt} \quad (3)$$

$$Q_{LOSS,MAX} = \frac{M_{LOSS}}{\int_0^t C_{UD}(t) dt} \quad (4)$$

where t is time, and C_U is the background-corrected concentration time series for the upstream slug at the upstream monitoring location. The corresponding gross gains are calculated by mass balance ($Q_{GAIN,MAX} = \Delta Q - Q_{LOSS,MAX}$ and $Q_{GAIN,MIN} = \Delta Q - Q_{LOSS,MIN}$). For cases where a positive mass loss is calculated in a net gaining segment, we assume that no tracer mass was lost (i.e., $Q_{LOSS} = 0$), and assign the net change in discharge for the reach to Q_{GAIN} [after *Payn et al*., 2009]. For cases where interpreted gross loss is smaller than observed net loss, we assume gross loss equals observed net loss, and zero gross gains. For cases of a positive mass loss in a net losing stream segment, we assume the tracer results are erroneous and omit them from analysis of long-term storage. We have not been able to identify specific sources of error in the data, nor do we have an ability to estimate the degree to which other observations were affected by these errors.

2.4. Short-Term Storage

[13] Although a parametric approach is common when analyzing stream solute breakthrough curve data (e.g., solving the transient storage equations of *Bencala and Walters* [1983]), mounting evidence suggests this approach is limited in its ability to characterize short-term storage due to high uncertainty and equifinality [e.g., *Mason et al*., 2012; *Lees et al*., 2000; *Wagner and Harvey*, 1997; C. A. Kelleher et al., Stream characteristics govern the importance of transient storage processes, submitted to *Water Resources Research*, 2013]. Therefore, we consider two analyses based on the observed breakthrough curves rather than a numerical modeling framework. These analyses include transient storage indices and temporal moment characteristics.

[14] The window of detection is a metric that is sensitive to both the physical system and measurement technique, and defines the boundary between short- and long-term storage [e.g., *Harvey et al*., 1996; *Harvey and Wagner*, 2000; *Ward et al*., 2013b]. We sampled tracer concentration until it was indistinguishable from background concentrations in the stream. Next, we calculated the window of detection as the time elapsed from the first detection of tracer in the stream above background noise to the time at which 99% of the recovered solute tracer signal has passed the observation location (hereafter t_{99}) [after *Ward et al*., 2013b; *Mason et al*., 2012]. We calculated the time elapsed between the observed breakthrough curve peak and t_{99}, signifying the time of apparent return to background tracer concentrations (hereafter the transient storage index, or TSI) [after *Mason et al*., 2012]. The t_{99} metric does not require the assumption of any distribution; it is calculated by trapezoidal integration of the observed time series. The TSI provides an indicator of transient storage (information contained in the tail of the breakthrough curve) relative to advective transport (information contained in the peak of the breakthrough curve) [*Mason et al*., 2012; *Harvey et al*., 1996]. The TSI is calculated as:

$$TSI = t_{99} - t_{peak} \quad (5)$$

[15] The TSI metric may be difficult to compare across reaches or different discharge conditions within a single reach. Therefore, we define:

$$\mathrm{TSI}_{\mathrm{norm}} = \mathrm{TSI}/t_{\mathrm{peak}} \quad (6)$$

[16] The $\mathrm{TSI}_{\mathrm{norm}}$ metric defines the number of advective timescales elapsed between t_{peak} and t_{99}, a metric previously used by *Gooseff et al*. [2007] to quantify relative residence times across multiple reaches and injections. The $\mathrm{TSI}_{\mathrm{norm}}$ metric quantifies the effect of processes other than advection on creating late-time tailing relative to the advective timescale, providing a metric that is independent of discharge or stream location.

[17] We also calculated temporal moments for the observed tracer breakthrough curves to quantify advective transport (first temporal moment, M_1), spreading (second central moment, μ_2), and tailing behavior (skewness, γ) of tracer in the study reaches [after *Gupta and Cvetkovic*, 2000; *Schmid*, 2003]. First the normalized concentration time series (*c(t)*) was calculated as

$$c(t) = \frac{C_b(t)}{\int_0^{t_{99}} C_b(t)dt} \quad (7)$$

where $C_b(t)$ is the observed tracer above background levels. This normalization yields a zeroth temporal moment (M_0) of unity for all cases (i.e., the area under each breakthrough curve is one; to remove differences due to changing slug masses and peak concentrations in-stream). Next, we calculated *n*-th-order temporal moments (M_n) and higher-order central moments ($_{\mu n}$) as

$$M_n = \int_0^{t_{99}} c(t)t^n dt, \quad (8)$$

and

$$\mu_n = \int_0^{t_{99}} c(t)(t - M_1)^n dt. \quad (9)$$

[18] Skewness was calculated by

$$\gamma = \frac{\mu_3}{\mu_2^{3/2}}. \quad (10)$$

[19] Finally, we normalized t by the modal advective time in the reach (based on time elapsed between upstream and downstream peak observations). Normalized time, t_{norm}, was calculated as

$$t_{\mathrm{norm}} = \frac{t}{t_{\mathrm{PEAK,DS}} - t_{\mathrm{PEAK,US}}} \quad (11)$$

where $t_{\mathrm{PEAK,DS}}$ and $t_{\mathrm{PEAK,US}}$ are the times at which the tracer peak passes the downstream and upstream loggers, respectively. The effect of this normalization is that each breakthrough curve peaks at a normalized time of one. The objective of this normalization was to compare the unique signature of each reach on the slug injection, and eliminate variation due to different slug masses and transport rates where transient storage across several streams with different breakthrough curves is normalized in this manner [after *Gooseff et al*., 2007]. This normalization is a comparison of system behavior that is not confounded by changes in the advective timescale or tracer mass. Throughout the manuscript, we use the subscript "norm" in addition to variables previously defined to denote analysis of the normalized breakthrough curve (e.g., γ_{norm}).

2.5. ANOVA for Metrics of Short- and Long-Term Storage

[20] We analyzed metrics of short- and long-term storage for both the observed and normalized breakthrough curves using a one-way Analysis of Variance (ANOVA). The objective of this analysis was to determine if the metrics describing short- and long-term storage differed significantly between the study reaches. We used a one-way ANOVA test to determine if individual reaches were statistically different based on the experimental window of detection (t_{99}), long-term (channel water balance) and short-term (TSI, temporal moments) storage. As applied to the three samples (i.e., the three study reaches), the ANOVA results indicate whether or not at least one sample mean is drawn from a different population than the others.

3. Results

3.1. Physical Hydrology

[21] The tracer-based discharge rates agreed well with the observations made at the catchment gauge, particularly for the lowest observed discharges (Figure 2). The largest deviations in dilution-gauging discharge estimates from the stream-gauge discharge estimates occurred during the highest discharge conditions (Figure 2b). The largest discharge values observed were during the first peak of the storm event were approximately 140 and 220% of the peak value observed at the H.J. Andrews Gauge (observed at the downstream and upstream ends of the downstream study reach, respectively). For example, the dilution gauging at the two downstream-most locations resulted in larger discharge than the gauge station at the discharge peaks (Figure 2). Although the gauge was most recently rebuilt in 1998, the gauge is calibrated using an unknown set of velocity rod measurements collected in the 1950s that established the stage-discharge relationship (D. Henshaw, Andrews forest streamflow calculation and rating curve summary, 2006, http://andrewsforest.oregonstate.edu/data/studies/hf04/rating_curve_history.pdf) and its accuracy at these discharge rates is unknown. During this study, discharge ranged from 21.5 to 434 L s^{-1} at the gauge station. For water year 2010 (1 October 2009 through 30 September 2010), the average discharge was 32.9 L s^{-1} (range 0.6–608 L s^{-1}); the flood of record is 2400 L s^{-1} [*Wondzell*, 2006].

[22] Overall, the stream discharge rapidly responded to rainfall. The two rainfall events that resulted in the hydrograph peaks represented approximately 13 cm of precipitation over a 2 day period, or a 1.25 year return interval storm event ($n = 53$ years) [*Voltz et al*., 2013]. The potentiometric surface of the valley bottom environment was also dynamic during the study period as it responded to the response to both rainfall on catchment hillslopes and dynamic flows in the stream. In the monitoring transects, the potentiometric surface rose in response to the storm

events and fell after the precipitation. At both locations, the stream gained water from the hillslope (Figure 3). The upstream transect shows a persistent potentiometric surface below that of the stream. The upstream transect is located where the active channel widens and the valley bottom topography is relatively flat and has a secondary channel. In contrast, the downstream transect is at a convergent location in the channel.

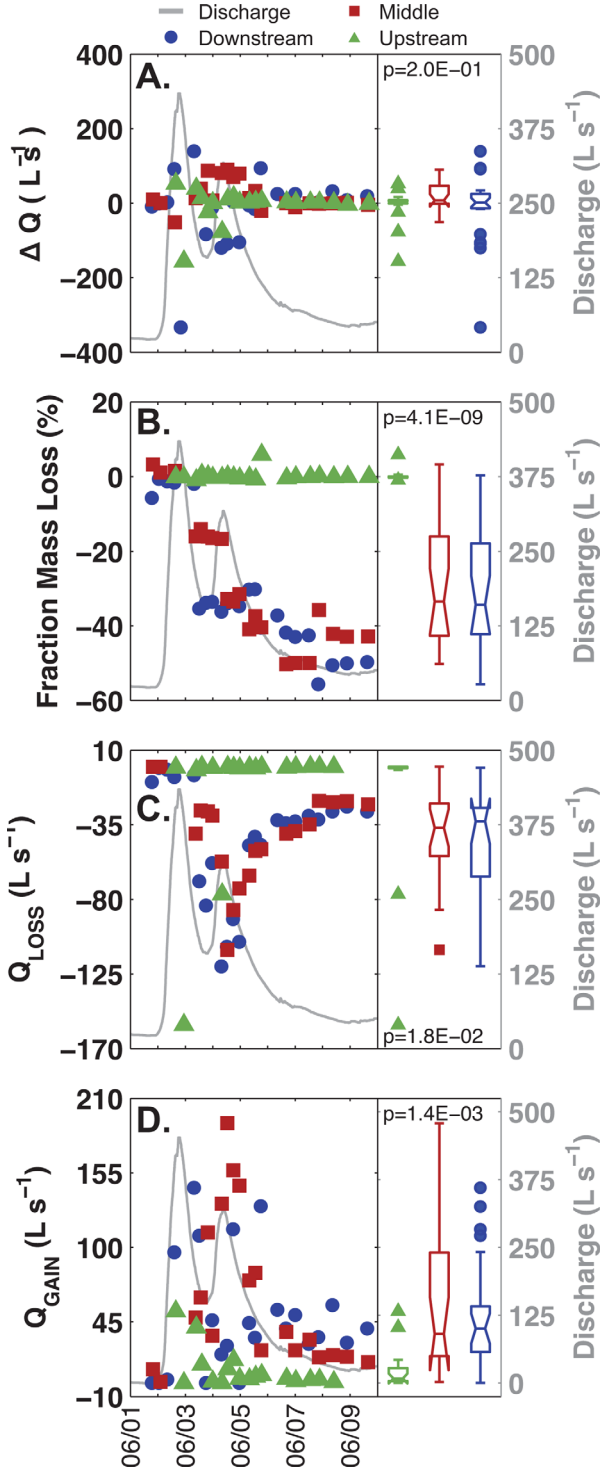

Figure 4.

3.2. Long-Term Storage

[23] Changes in discharge at the gauge station averaged 0.46% of discharge (range 0.0–2.5%) during the integration periods for individual dilution gauging measurements. Given this small change over short timer periods, we assumed the steady state flow conditions were satisfactorily met for individual dilution gauging events, and that our dilution gauging was valid despite the dynamics in response to rainfall. Net changes in discharge demonstrate that the stream was generally gaining during the study period (58% of all observations), although each segment exhibited net losing behavior during multiple discharge conditions (Figure 4a).

[24] The fraction of slug mass lost within a given reach, a fundamental quantity used to derive long-term storage fluxes from solute tracer data, varied in a regular pattern for most study reaches with rising and recessional limbs of the hydrograph (Figure 4b). For 5 of the 72 tracer time series, a positive mass loss was observed in a net losing segment and omitted from further analysis for long-term storage. In all locations, mass losses from prestorm conditions through the first rising limb and about half of the first falling limb (i.e., the first five slug injections) are negligible. Approximately halfway through the first falling limb, a substantial shift in tracer mass loss was observed in the downstream and middle reaches.

[25] During the second rising limb, mass loss remained approximately constant in each study reach. Finally, during the second recession, mass loss in the middle and downstream reaches slowly increased, and was approximately constant for the final three tracer injections. Peak changes in the fluid electrical conductivity averaged 58.2 μS/cm (range 11.6–158.3 μS/cm), providing a signal that was at least an order of magnitude above the variability in background fluid electrical conductivity during the storm events.

[26] We analyzed long-term storage using the frameworks of both maximum dilution (gain before loss) and maximum tracer mass loss (loss before gains). Spatial and temporal patterns for both were similar. We present results only for the condition of maximum dilution, as is the

Figure 4. (a) Net changes in flow, ΔQ, (b) tracer mass loss, (c) gross losses (Q_{LOSS}), and (d) gross gain (Q_{GAIN}) for each study reach. Boxplots and one-way ANOVA results summarize long-term storage (tracer mass that does not return to the stream channel within the window of detection) for each study reach. Long-term storage data and boxplots are associated with the left-hand Y axes; discharge with the right-hand y axes. ANOVA results indicate the probability that at least one sample mean is drawn from a population with a different mean than the others. If tapered sections of the boxplots do not overlap, the two medians are different at the 5% significance level. For example, in Figure 4c, the tapered sections for the upstream box does not overlap with the middle nor downstream reach boxes, so it is significantly different than both of those. Tapered sections for the middle and downstream boxes do overlap, so they are not significantly different. Dates are MM/DD in 2010.

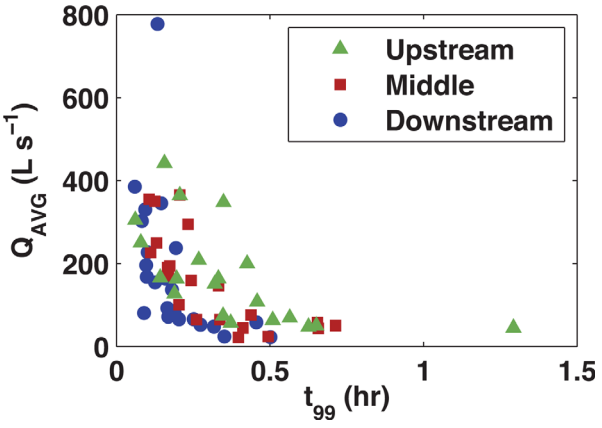

Figure 5. Tracer window of detection (interpreted here at the time elapsed until 99% of the recovered mass is observed, t_{99}) was inversely related to discharge in all three study reaches.

practice for recent studies considering hydrologic turnover in stream networks [e.g., *Covino et al*., 2011]. Gross losses of channel water remain small or zero during the first rising limb in all reaches (Figure 4c). Gross losses in the downstream and middle reaches initially increased during the first falling limb, and then decreased as the hydrograph reached the trough between storm flow peaks. Losses in downstream and middle reaches increased during the second rising limb, and then slowly decreased as the hydrograph receded to base flow. Gross gains to the stream for the middle and downstream reaches generally increased during the rising limbs and fell during the receding limbs (Figure 4d). In the downstream reach, gross gains of channel water increased briefly then decreased during the first falling limb. In the middle reach, gains slowly increased and then decreased during the first falling limb. In all study segments, the gross gains and losses reached a nearly constant magnitude during the second falling limb of the hydrograph, yet exhibit varied responses during the storm event (Figures 4c and 4d).

3.3. Short-Term Storage

[27] In this study, t_{99} varied between 0.06 and 1.3 h for the study reaches, with maximum values corresponding to low in-stream discharges (Figures 5 and 6a). TSI ranged from 0.043 to 1.3 h (mean 0.26 h) with larger values corresponding to low in-stream discharges (Figure 6c). Small increases in magnitudes of TSI were observed during the temporary recession in discharge between storm peaks in the upstream and middle reaches. Mean arrival time (M_1) was inversely related to discharge with the largest values (slowest modal transport velocity) associated with the lowest discharges (Figure 6e). Temporal variance of the tracer (μ_2) decreased during the high discharge conditions with the largest values observed during the low discharge conditions (Figure 6g). Conversely, skewness (γ) increased with discharge in the upstream reach (Figure 6i). Both the middle and downstream reaches exhibited nearly constant γ throughout the study period. These results agree with those reported by *Ward et al*. [2013b] along a gradient in base flow discharge where t_{99} and discharge were found to be important controls on metrics of short-term storage.

[28] Analysis of normalized breakthrough curves provides an assessment independent of t_{99} and peak concentration in-stream. For the normalized breakthrough curves, t_{99} is nearly constant throughout the study period for the downstream and upstream reaches, and increased slightly in the middle reach (Figure 6b). Both TSI_{norm} and $M_{1,norm}$ exhibited similar trends (Figures 6d and 6f). The number of advective timescales elapsed between the peak and the last detection of tracer, TSI_{norm}, ranged from 1.7 to 17.7 with small TSI_{norm} values corresponding to small values of t_{99}. In contrast to the μ_2 and γ trends for observed breakthrough curves, the normalized metrics exhibited more constant values through time, though noise is present in the relationships (Figures 6h and 6j). All observed and normalized solute tracer breakthrough curves are presented as supporting information Figure 1.

3.4. Comparison of Short- and Long-Term Storage Between Reaches

[29] We tested for significant differences among the different study reaches using a one-way ANOVA for metrics of both short- and long-term storage (95% confidence level; $p < 0.05$ is significant; see boxplots in Figures 4 and 6). ANOVA results, as calculated here, indicate whether or not at least one study reach was significantly different from the others. First, we analyzed the observed breakthrough curves. For long-term storage, the fraction of slug mass lost was significantly different for the upstream study reach ($p < 0.0001$). This difference was maintained for Q_{LOSS} ($p = 0.018$) and Q_{GAIN} ($p = 0.0014$). Sample population means were not significantly different for ΔQ ($p = 0.20$). For short-term storage, significant differences exist based on observed breakthrough curves for t_{99} ($p = 0.0088$; downstream reach is significantly different), TSI ($p = 0.0051$; downstream reach is significantly different), and γ ($p < 0.0001$; all three reaches are significantly different from each other). No significant differences were found for M_1 ($p = 0.33$) or μ_2 ($p = 0.39$). Next, we analyzed the normalized breakthrough curves, finding significant differences for $t_{99,norm}$ ($p < 0.0001$; all three reaches are significantly different from each other), TSI_{norm} ($p < 0.0001$; all three reaches are significantly different from each other), $M_{1,norm}$ ($p = 0.0019$; downstream reach is significantly different from the other two reaches), $\mu_{2,norm}$ ($p = 0.012$; downstream reach is significantly different from the other two reaches), and γ_{norm} ($p < 0.0001$; all three reaches are significantly different from each other).

3.5. The Window of Detection as a Control on Interpreting Short- and Long-Term Storage

[30] Mass losses in the upstream and middle reaches were nearly independent of t_{99}, while the downstream reach exhibited variability (Figure 7a). Short-term storage was strongly related to t_{99} throughout the storm event and recession for both the observed (left column in Figure 7) and normalized (right column in Figure 7) breakthrough curves. TSI increases linearly with t_{99}, with the greatest time elapsed between the advective timescale and t_{99} occurring during the slowest transport times (Figures 7c and 7d). We found increasing M_1 with increasing t_{99} (Figures 7e and 7f). Temporal variance (Figures 7g and 7h)

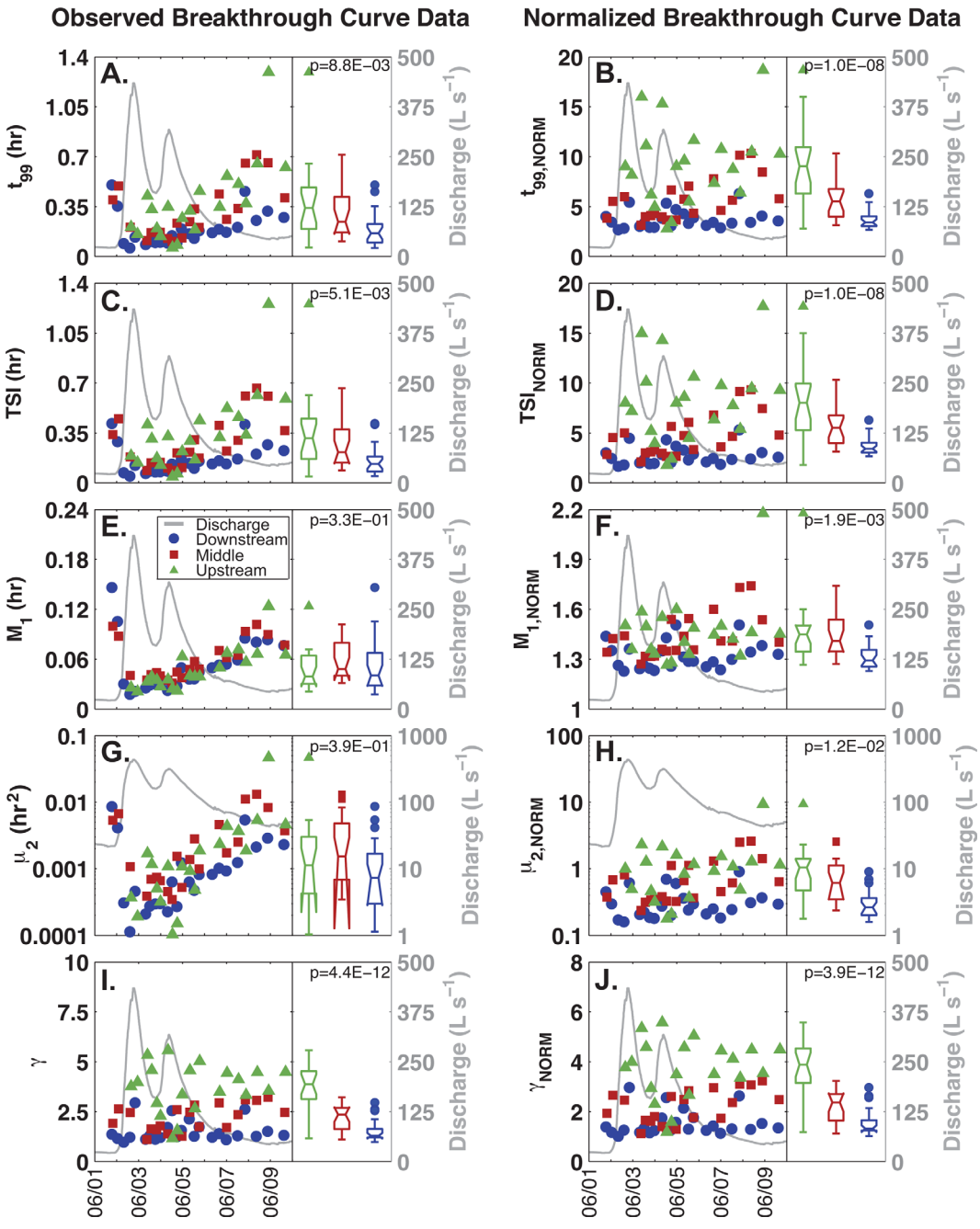

Figure 6. Metrics of short-term storage for (a, c, e, g, and i) observed and (b, d, f, h, and j) normalized breakthrough curves. Left-hand plots show metrics of short-term storage for each study reach through time. Short-term storage data and boxplots are associated with the left-hand *Y* axes; discharge with the right-hand *y* axes. ANOVA results indicate the probability that at least one sample mean is drawn from a population with a different mean than the others. If tapered sections of the boxplots do not overlap, the two medians are different at the 5% significance level. For example, no tapered sections overlap in Figure 6j, indicating significant differences between all three reaches. Dates are MM/DD in 2010 on the *X* axis.

and skewness (Figures 7i and 7j) increase with t_{99} suggesting that processes other than advection in the stream channel (e.g., dispersion) have a greater effect on the solute signal when they have more time to act on that signal. If the spreading and tailing are attributed to hyporheic exchange, this suggests the observable timescales of subsurface processes are primarily affected by the advective velocity of the stream.

4. Discussion

4.1. Linking Short- and Long-Term Storage With Valley Bottom Hydrology

[31] There was little variation in the direction of riparian hydraulic gradients lateral to the valley bottom throughout the storm events of this study (Figure 3, Upstream Transect). Persistent losing conditions observed at the upstream

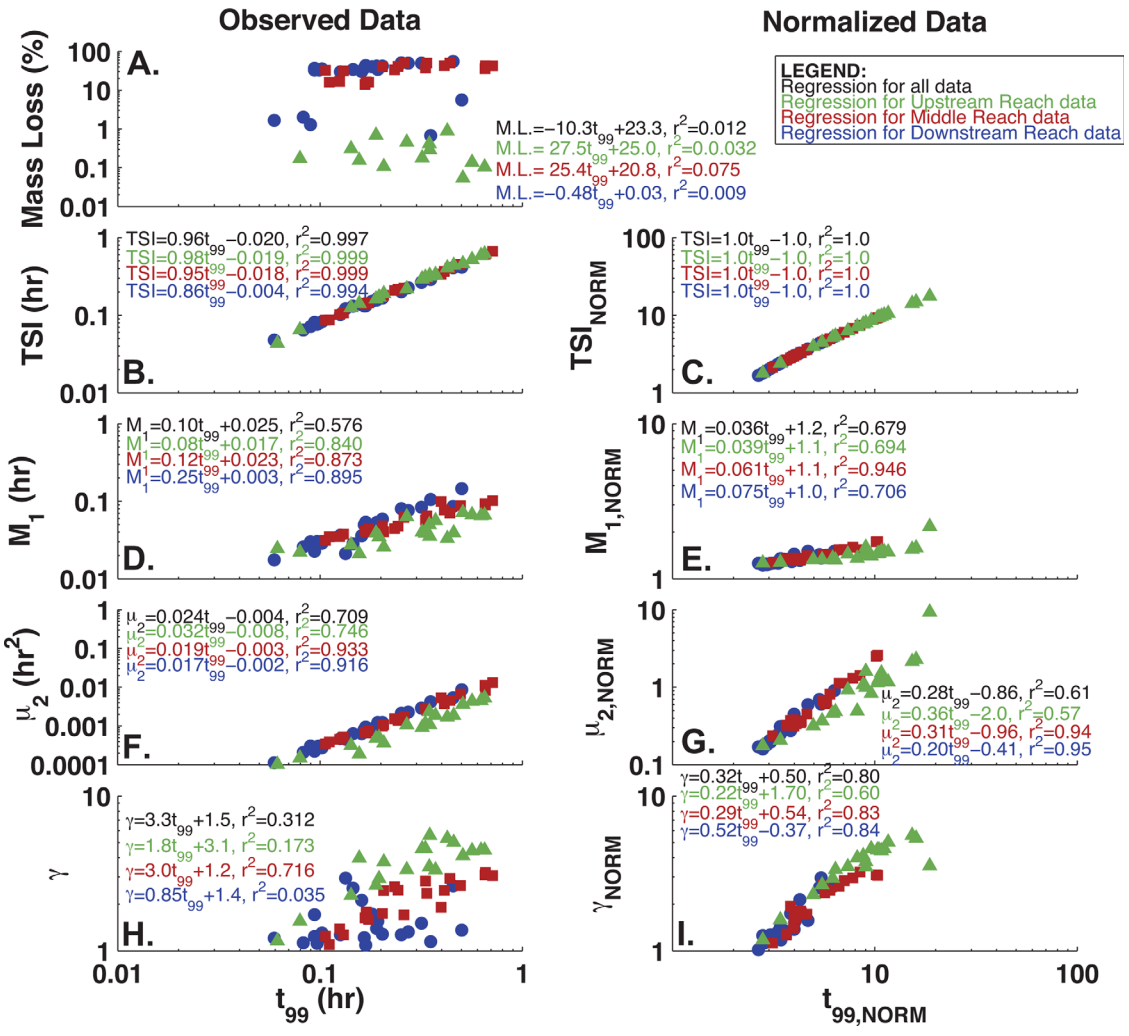

Figure 7. Short-term storage in both (left) observed and (right) normalized breakthrough curves are strongly related to the window of detection (t_{99}, $t_{99,norm}$). Metrics of short-term storage considered here include (a) tracer mass loss, (b and c) transient storage index, (d and e) mean arrival time, (f and g) temporal variance, and (h and i) skewness.

transect are inconsistent with the conceptual models that predict increasing hydraulic gradients toward the stream during storm events and suppressing hyporheic flow [*Hakenkamp et al*., 1993; *Hynes*, 1983; *Meyer et al*., 1988; *Palmer*, 1993; *Vervier et al*., 1992; *White*, 1993]. The stream appears to always lose water to the subsurface in some locations, even when the stream stage is rising (Figure 3, Upstream Transect). We interpret this as evidence of persistent hyporheic exchange driven by local geomorphology, and as a simultaneous gain of water and loss of water along hyporheic flow paths from the stream channel perspective.

[32] Previous studies in the same watershed also demonstrate that this valley-bottom hydrology behavior is not unique to this study or event [see *Voltz et al*., *2013*; *Wondzell*, 2006; *Wondzell et al*., 2010]. *Voltz et al*. [2013] showed in detail that the gradients in and adjacent to the stream channel change very little in response to the storm events in the highly instrumented section of the middle reach (Figure 1c). Their study further found that most locations in the WS1 valley bottom were dominated by down-valley hydraulic gradients (parallel to the stream) as opposed to cross-valley gradients (perpendicular to the stream) upon which the majority of current conceptual models are based. During the storm event, *Voltz et al*. [2013] report that near-stream hydraulic gradients in some locations even turn away from the stream channel, increasing the movement of water and tracer from the stream to the aquifer.

[33] We hypothesize the persistent hyporheic flow paths observed at the upstream transect in the present study (Figure 3) are due to the location of this transect near a riffle and widening section of the valley bottom. In a nearby steep mountain catchment (Watershed 3, < 1 km from WS1 in the HJ Andrews Experimental Forest), *Ward et al*. [2012] found that the physical extent of stream water in the aquifer during base flow recession was largely invariant, and that geomorphology was the primary control on stream-aquifer interactions in this system. There is a growing body of literature suggesting that valley-bottom geology and near surface morphology (e.g., hillslopes, valley bottom width, underlying bedrock profile and alluvial

deposit depth) are the dominant controls on stream-aquifer interactions in steep headwater streams [e.g., *Kasahara and Wondzell*, 2003; *Wondzell*, 2006; *Wondzell et al*., 2010; *Payn et al*., 2012; *Ward et al*., 2012, 2013a]. The present study suggests that geomorphology of the individual stream reaches in combination with the hillslopes discharging to the valley bottom modifies solute tracer time series in a predictable way, scaled by the overall advective travel time in the reach. The magnitude of metrics describing the short-term storage increases with increasing t_{99}; for example, skewness grows with increasing t_{99} because there is more time for processes other than advection to act on the signal.

[34] Conceptually, experiments with larger t_{99} should exhibit increased μ_2 and γ, because short-term storage processes would have more time to act on the solute tracer signals. The novel storm-event data from this study confirm this relationship for both observed and normalized breakthrough curves (Figure 7). For longer advective timescales, we found longer mean travel times (Figures 7e and 7f). Positive relationships between t_{99} and higher-order central moments (Figures 7f–7i) suggest that increased short-term storage (evidenced by increased spreading and asymmetric tailing) occurs during the lowest discharge conditions. These t_{99} patterns are also a function of the channel hydraulics controlled by the geomorphology of the valley bottom. However, we posit that the different slopes observed between γ and t_{99} are indicative of changes in the stream and valley bottom morphology. For example, the relationship between discharge and channel structure in the upstream reach may allow the active stream channel to temporarily access portions of the riparian valley bottom that include many roughness elements, that increase surface transient storage (e.g., fallen logs, debris jams, shrubs, and grasses). We attribute the incorporation of these elements into the active channel as the source of the observed relationship between t_{99} and γ surface transient storage. Inherent in this attribution is that these storage processes affect transient storage (indicated by a larger γ), but not advection nor longitudinal dispersion (which would appear in values for M_1 and μ_2, respectively).

4.2. Stream Reaches Provide Characteristic Modification to Solute Signals Independently of In-Stream Discharge Rate

[35] The first major precipitation event caused a shift in long-term storage that did not return to pre-storm conditions during the study. While hysteretic behavior of hillslope-riparian-stream interactions has been reported [e.g., *McGlynn and McDonnell*, 2003; *McGlynn et al*., 2004*; McGuire and McDonnell*, 2010], these studies have not been extended to account for the behavior within the riparian and hyporheic zones. This shift in long-term storage is particularly evident in the patterns in mass loss, where the middle and downstream reaches show increasing mass loss during the storm event and its recession. These mass losses represent substantial increases in Q_{LOSS} and corresponding increases in Q_{GAIN} during the second peak of the storm event. Furthermore, the storm caused a shift in short-term storage interpreted from recovered in-stream tracer. The valley-bottom hydrology was not highly dynamic during the storm event based on ground water elevations alone. However, with the evidence of the tracer studies, it is clear that both short- and long-term storage were highly variable during the storm events. Thus, the exchange of water between streams and their aquifers is highly dynamic during storm events and may not be apparent to investigations solely relying on valley-bottom ground water elevations. No notable, irreversible changes in the physical morphology of the system were observed during the storm event (e.g., hillslope failures, log falls) to explain this change in storage. Changes in stage did result in different extents of the valley bottom becoming active parts of the channel during the different periods of the study.

[36] In WS1 and across a large range of discharges, the normalized breakthrough curves showed that each of the study reaches imparted a unique modification to the injected solute tracer. While there is not a ubiquitous correlation of all normalized breakthrough curves at an individual reach, we found unique storage modifications within each reach that were significantly different from one another. This is similar to storage dynamics observed by *Zarnetske et al*. [2007], who concluded that unique reach morphologies can act as stronger modifiers of water storage dynamics than orders-of-magnitude variability in discharge. Further, the observed relationships between discharge and all short-term storage metrics suggests that the same suite of flow paths is affecting the in-stream solute signal during all flow conditions, because the effect of these flow paths on the tracer signal varies as a function of t_{99} (i.e., the window of detection for each tracer study). More formally, the process domain (i.e., the region in space and time over which the morphologic structure of the stream influences stream hydraulics [*Montgomery*, 1999]) is nearly constant through space and time based on our normalized solute tracer data. The combination of morphology and discharge is unique to each tracer study and gives rise to a unique window of detection, which confounds the interpretation of short- and long-term storage in our study and others [e.g., *Ward et al*., 2013b; *Drummond et al*., 2012].

4.3. A Dynamic Perceptual Model of the Hillslope-Riparian-Hyporheic-Stream Continuum

[37] To explain observed metrics of short- and long-term storage, we pose a three-dimensional (3-D), dynamic, perceptual model as an explanation of the observed patterns of metrics describing short- and long-term storage that were observed in this study. The perceptual model is a qualitative representation of dominant processes that are critical to a description of hydrological system response, and is based on subjective understanding of hydrological processes occurring at the field site [e.g., *Sivapalan*, 2003; *Wagener et al*., 2007]. We present our perceptual model of the WS1 hillslope-riaparian-hyporheic-stream continuum to explain the field observations that do not fit within existing conceptual models. Further this conceptual mode serves to integrate our understanding of the hydrological processes in the sense of, for example, *McGlynn et al*. [1999], acknowledging that continued study is often coupled with refinement and revision of such perceptual models [*McGlynn et al*., 2002]. Although the perceptual model includes the major drivers and feedbacks of the system, the magnitudes of each are expected to be heterogeneous in space (e.g., between study reaches).

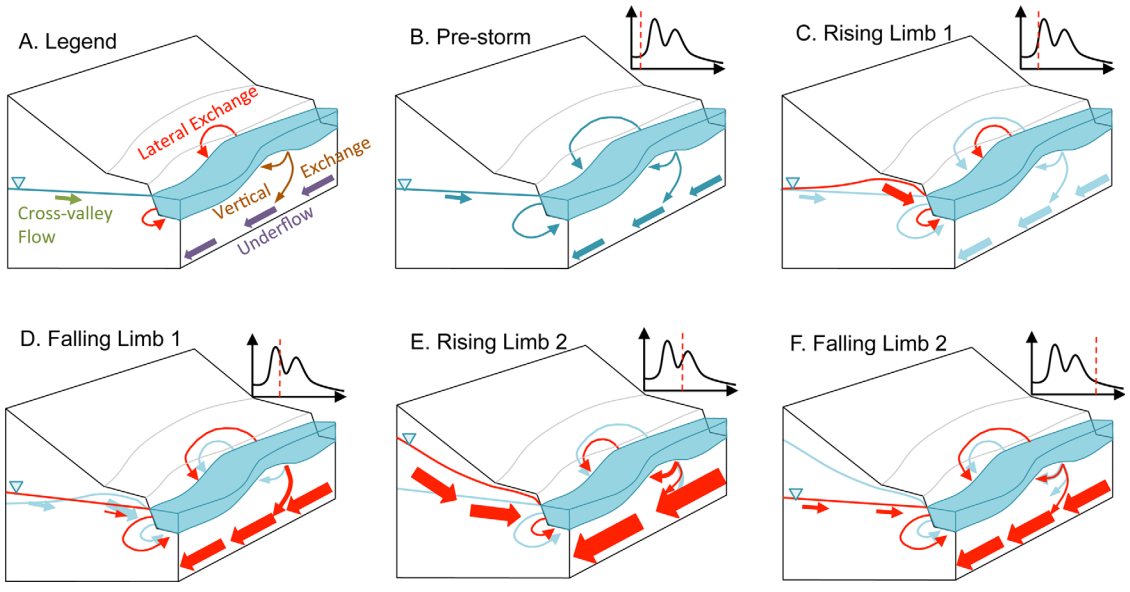

Figure 8. Perceptual model of hillslope-riparian-hyporheic-stream continuum during rising and falling limbs of storm event. (a) Legend identifying processes represented in the perceptual model. (b) Pre-event perceptual model. (c–f) Changes in processes through the rising and falling limbs during the study. Processes that change from the previous plot are represented in red, while the processes from the previous plot are shown in the faded blue color. Inset represents the location of each panel through the storm event.

[38] Our perceptual model of WS1 represents the prestorm through recession limb period captured by this study, and the variable flow conditions across the hillslope-riparian-hyporheic-stream continuum (Figure 8). As the first storm event occurs and the initial rising limb develops in the stream, the riparian zone responds rapidly, compressing hyporheic flow path networks and creating generally gaining conditions evidenced by the low mass loss in all reaches during the prestorm and first rising limb (Figure 8c). Following the cessation of the first storm event and during the first falling limb (Figure 8d), the hydraulic gradients from the hillslope and riparian zone to the stream decrease (Figure 3), allowing increased lateral extent of hyporheic flow paths and increased tracer mass loss. The down-valley underflow increases as a result of the catchment response to the precipitation, because the hillslopes begin discharging to the riparian zone, which is dominated by down-valley hydraulic gradients in WS1 [*Voltz et al.*, 2013]. Across the variable flow conditions, the mass lost from the stream channel is more likely to remain in underflow rather than return to the stream, which explains the increased mass loss during the first falling limb of the study (Figure 2). During the rising limb of the second precipitation event (Figure 8e), the hillslopes and riparian zones (with increased antecedent moisture levels due to the first precipitation event) respond rapidly, increasing hydraulic gradients toward the stream. This compresses hyporheic exchange pathways in accordance with several existing conceptual models [e.g., *Hynes*, 1983; *Meyer et al.*, 1988; *Vervier et al.*, 1992; *Hakenkamp et al.*, 1993; *Palmer*, 1993; *White*, 1993] and explains the plateau in tracer mass loss (Figure 4). During the second rising limb, the underflow is maintained [*Voltz et al.*, 2013], transporting tracer lost from the stream down-valley in the aquifer, and eventually returning the flow and tracer to the stream downstream of the study reach. Finally, following the cessation of the second storm event (Figure 8f), the hydraulic gradients from the hillslope to stream relax, allowing the expansion of the hyporheic zone. The underflow remains high during this second recession period, because the upstream catchment is still relaxing back to prestorm conditions and discharging to this convergent location near the catchment outlet. This extended relaxation period explains why the observed tracer behavior does not return to prestorm conditions (e.g., very low tracer mass loss) during our study period despite the return of discharge to prestorm magnitudes (Figure 2).

5. Conclusions

[39] We collected a unique data set of conservative solute tracer transport before, during, and after a major storm event in a headwater mountain stream. These data characterize both short- and long-term storage in the stream and reveal an improved understanding of how water and solutes move through the stream network during storm events. The tracer tests provide evidence of short- and long-term storage, both representing some amount of interaction between the stream and groundwater at the reach-averaged scale. We use a variety of metrics to describe the solute tracer breakthrough curves (e.g., TSI, t_{99}), and we note here that these are descriptors only; that do not isolate cause-effect relationships for watershed processes and storage dynamics. Further, the observations of the valley-bottom head gradients alone indicate magnitudes and directions of exchange, but are limited in space. The interpretations of tracer tests alone are complicated because they span a range of spatial scales. However, both tracer studies and water table observations demonstrate dynamic hydrological fluxes during storm events. Given that hydrodynamics are recognized as a significant control on biological and chemical systems in streams

and their ground waters [after *Battin*, 1999, 2000; *Zarnetske et al*., 2011; *Ward et al*., 2011], the decrease of t_{99} with increasing discharge suggests a decreased potential for hyporheic and riparian biogeochemical cycling to affect in-stream signatures. It is unlikely that static conceptual models are sufficient to explain the sources of observed in-stream biological and chemical processes during dynamic flow conditions. Therefore, we developed a new conceptual model for the dynamics of hillslope-riparian-hyporheic-stream continuum at the site across storm events. Still, further work is needed, because neither technique in this study nor the combination of them fully captures the time-variable 3-D exchanges occurring between the stream and its aquifer across the range of spatial and temporal scales.

[40] Overall, this study demonstrates that: (1) metrics of short- and long-term storage were highly variable with stream discharge, largely due to variation in the tracer-based window of detection; (2) characteristic modifications of solute tracer signals exist in different study reaches independent of stream discharge and can be predominantly controlled by valley-bottom morphology; (3) localized losing conditions were consistently observed in certain locations even during the rising limb of the storm hydrograph, demonstrating local hyporheic flow paths that persist through strongly gaining conditions at the valley-bottom scale; (4) short- and long-term storage are complimentary descriptions of stream water and solute transport, partitioned by the window of detection; (5) stream discharge responds to storm events and recovers from them over a shorter timescale than metrics of short- and long-term storage recover; (6) the exchange of water between streams and their aquifers is highly dynamic during storm events and may not be apparent to investigations solely relying on valley-bottom ground water elevations; and (7) down-valley flux in the subsurface is an important component of stream-aquifer interactions that is not represented in many conceptual models of riparian hydrology. Understanding the fate of water and solutes in headwater streams requires in-depth understanding of riparian zone hydrology. Short- and long-term storage are complementary processes that define how solute signals at the upstream end of a reach are translated to the downstream end, with implications for solute fate and transport at the network scale.

[41] **Acknowledgments.** Climate and stream discharge data were provided by the Forest Science Data Bank, a partnership between the Department of Forest Science, Oregon State University, and the U.S. Forest Service Pacific Northwest Research Station, Corvallis, Oregon. Significant funding for these data was provided by the National Science Foundation's Long-Term Ecological Research program (DEB 08–23380), US Forest Service Pacific Northwest Research Station, and Oregon State University. This manuscript is based upon work supported by the National Science Foundation's Hydrologic Sciences program, under grant EAR-0911435. JZ acknowledges additional support from the Yale Institute for Biospheric Studies. Any opinions, findings, and conclusions or recommendations expressed in this material are those of the authors and do not necessarily reflect the views of the National Science Foundation or the H. J. Andrews Experimental Forest. The authors thank the reviewers for constructive feedback that improved the quality of this manuscript.

References

Battin, T. (1999), Hydrologic flow paths control dissolved organic carbon fluxes and metabolism in an alpine stream hyporheic zone, *Water Resour. Res.*, *35*(10), 3159–3169, doi:10.1029/1999WR900144.

Battin, T. (2000), Hydrodynamics is a major determinant of streambed biofilm activity: From the sediment to the reach scale, *Limnol. Oceanogr.*, *45*, 1308–1319, doi:10.4319/lo.2000.45.6.1308.

Bencala, K., and R. Walters (1983), Simulation of solute transport in a mountain pool-and-riffle stream: A transient storage model, *Water Resour. Res.*, *19*(3), 718–724.

Boulton, A. J., S. Findlay, P. Marmonier, E. H. Stanley, and H. M. Valett (1998), The functional significance of the hyporheic zone in streams and rivers, *Annu. Rev. Ecol. Syst.*, *29*(1), 59–81.

Brunke, M., and T. Gonser (1997), The ecological significance of exchange processes between rivers and groundwater, *Freshwater Biol.*, *37*, 1–33.

Cardenas, M. B. (2009), Stream-aquifer interactions and hyporheic exchange in gaining and losing sinuous streams, *Water Resour. Res.*, *45*, W06429, doi:10.1029/2008WR007651.

Castro, N. M., and G. M. Hornberger (1991), Surface-subsurface water interactions in a alluviated mountain stream channel, *Water Resour. Res.*, *27*(7), 1613–1621.

Covino, T., B. McGlynn, and J. Mallard (2011), Stream-groundwater exchange and hydrologic turnover at the network scale, *Water Resour. Res.*, *47*, W12521, doi:10.1029/2011WR010942.

Day, T. (1977), Field procedures and evaluation of a slug dilution gauging method in mountain streams, *N. Z. J. Hydrol.*, *16*(2), 113–133.

Drummond, J., T. P. Covino, A. Aubeneu, D. Leong, S. Patil, R. Schumer, and A. Packman (2012), Effects of solute breakthrough curve tail truncation on residence time estimates: A synthesis of solute tracer injection studies, *J. Geophys. Res.*, *117*, G00N08, doi:10.1029/2012JG002019.

Dyrness, C. T (1969), Hydrologic properties of soils on three small watersheds in the western Cascades of Oregon, Res. Note PNW-111, Pac. Northwest For. and Range Exp. Stn., For. Serv., U.S. Dep. of Agric., Portland, Oreg.

Fischer, H. B., E. J. List, R. C. Y. Koh, J. Imberger, and N. H. Brooks (1979), *Mixing in Inland and Coastal Waters*, Academic, San Diego, Calif.

Florkowski, T., T. G. Davis, B. Wallander, and D. R. L. Prabhakar (1969), The measurement of high discharges in turbulent rivers using tritium tracer, *J. Hydrol.*, *8*, 248–261.

Francis, B. A., L. K. Francis, and M. B. Cardenas (2010), Water table dyamics and groundwater-surface water interactions during filling and draining of a large fluvial island due to dam-induced river stage fluctuations, *Water Resour. Res.*, *46*, W07513, doi:10.1029/2009WR008694.

Gooseff, M. N., R. O. Hall Jr., and J. L. Tank (2007), Relating transient storage to channel complexity in streams of varying land use in Jackson Hole, Wyoming, *Water Resour. Res.*, *43*, W01417, doi:10.1029/2005WR004626.

Gooseff, M. N., R. A. Payn, J. P. Zarnetske, W. B. Bowden, J. P. McNamara, and J. H. Bradford (2008), Comparison of in-channel mobile-immobile zone exchange during instantaneous and constant rate stream tracer additions: Implications for design and interpretation of non-conservative tracer experiments, *J. Hydrol.*, *357*(1–2), 112–124.

Gu, C., G. M. Hornberger, A. L. Mills, and J. S. Herman (2008), Influence of stream-aquifer interactions in the riparian zone on NO3-flux to a low-relief coastal stream, *Water Resour. Res.*, *44*, W11432, doi:10.1029/2007WR006739.

Gupta, A., and V. Cvetkovic (2000), Temporal moment analysis of tracer discharge in streams: Combined effect of physicochemical mass transfer and morphology, *Water Resour. Res.*, *36*(10), 2985–2997.

Hakenkamp, C. C., H. M. Valett, and A. J. Boulton (1993), Perspectives on the hyporheic zone: Integrating hydrology and biology. Concluding remarks, *J. N. Am. Benthol. Soc.*, *12*(1), 94–99.

Harvey, J., and K. Bencala (1993), The effect of streambed topography on surface-subsurface water exchange in mountain catchments, *Water Resour. Res.*, *29*(1), 89–98.

Harvey, J. W., and B. J. Wagner (2000), Quantifying hydrologic interactions between streams and their subsurface hyporheic zones, in *Streams and Ground Waters*, edited by J. B. Jones and P. J. Mulholland, pp. 3–44, Academic, San Diego, Calif.

Harvey, J. W., B. J. Wagner, and K. E. Bencala (1996), Evaluating the reliability of the stream tracer approach to characterize stream-subsurface water exchange, *Water Resour. Res.*, *32*(8), 2441–2451.

Hynes, H. (1983), Groundwater and stream ecology, *Hydrobiologia*, *100*(1), 93–99.

Jackman, A. P., R. A. Walters, V. C. Kennedy (1984), Transport and concentration controls for chloride, strontium, potassium and lead in Uvas Creek, a small cobble-bed stream in Santa Clara County, California, USA: 2. Mathematical modeling, *J. Hydrol.*, *75*(1–4), 111–141.

Jencso, K. G., and B. L. McGlynn (2011), Hierarchical controls on runoff generation: Topographically driven hydrologic connectivity, geology, and vegetation, *Water Resour. Res.*, *47*, W11527, doi:10.1029/2011WR010666.

Jencso, K. G., B. L. McGlynn, M. N. Gooseff, K. E. Bencala, and S. M. Wondzell (2010), Hillslope hydrologic connectivity controls riparian groundwater turnover: Implications of catchment structure for riparian

buffering and stream water sources, *Water Resour. Res.*, *46*, W10524, doi:10.1029/2009WR008818.

Kasahara, T., and S. M. Wondzell (2003), Geomorphic controls on hyporheic exchange flow in mountain streams, *Water Resour. Res.*, *39*(1), 1005, doi:10.1029/2002WR001386.

Kennedy, V. C., A. P. Jackman, S. M. Zand, G. W. Zellweger, and R. J. Avanzino (1984), Transport and concentration controls for chloride, strontium, potassium and lead in Uvas Creek, a small cobble-bed stream in Santa Clara County, California, USA: 1. Conceptual model, *J. Hydrol.*, *75*(1–4), 67–110.

Krause, S., D. M. Hannah, J. H. Fleckenstein, C. M. Heppell, D. Kaeser, R. Pickup, G. Pinday, A. L. Robertson, and P. J. Wood (2011), Interdisciplinary perspectives on processes in the hyporheic zone, *Ecohydrology*, *4*(4), 481–499.

Larkin, R. G., and J. M. Sharp (1992), On the relationship between river-basin geomorphology, aquifer hydraulics, and ground-water flow direction in alluvial aquifers, *Bull. Geol. Soc. Am.*, *104*(12), 1608–1620.

Lees, M., L. A. Camacho, and S. Chaptra (2000), On the relationship of transient storage and aggregated dead zone models of longitudinal solute transport in streams, *Water Resour. Res.*, *36*(1), 213–224.

Mason, S. J. K., B. L. McGlynn, and G. C. Poole (2012), Hydrologic response to channel reconfiguration on Silver Bow Creek, Montana, *J. Hydrol.*, *438–439*, 125–136.

McGlynn, B. L., and J. J. McDonnell (2003), Quantifying the relative contributions of riparian and hillslope zones to catchment runoff, *Water Resour. Res.*, *39*(11), 1310, doi:10.1029/2003WR002091.

McGlynn, B.L., J. J. McDonnel, J. B. Shanley, and C. Kendall (1999), Riparian zone flowpath dynamics during snowmelt in a small headwater catchment, *J. Hydrol.*, *222*, 75–92.

McGlynn, B. L., J. J. McDonnel, and D. D. Brammer (2002), A review of the evolving perceptual model of hillslope flowpaths at the Maimai catchments, New Zealand, *J. Hydrol.*, *257*, 1–26.

McGlynn, B. L., J. J. McDonnel, J. Seibert, and C. Kendall (2004), Scale effects on headwater catchment runoff timing, flow sources, and groundwater-streamflow relations, *Water Resour. Res.*, *40*, W07504, doi:10.1029/2003WR002494.

McGuire, K. J., and J. J. McDonnel (2010), Hydrological connectivity of hillslopes and streams: Characteristic time scales and nonlinearities, *Water Resour. Res.*, *46*, W10543, doi:10.1029/2010WR009341.

Meyer, J. L., W. H. McDowell, T. L. Bott, J. W. Elwood, C. Ishizaki, J. M. Melack, B. L. Peckarsky, B. J. Peterson, and P. A. Rublee (1988), Elemental dynamics in streams, *J. N. Am. Benthol. Soc.*, *7*(4), 410–432.

Montgomery, D. R. (1999), Process domains and the river continuum, *J. Am. Water Resour. Assoc.*, *35*(2), 397–410.

Nowinski, J. D., M. B. Cardenas, A. F. Lightbody, T. E. Swanson, and A. H. Sawyer (2012), Hydraulic and thermal response of groundwater-surface water exchange to flooding in an experimental aquifer, *J. Hydrol.*, *472–473*, 184–192.

Palmer, M. A. (1993), Experimentation in the hyporheic zone: Challenges and prospectus, *J. N. Am. Benthol. Soc.*, *12*(1), 84–93.

Payn, R. A., M. N. Gooseff, D. A. Benson, O. A. Cirpka, J. P. Zarnetske, W. B. Bowden, J. P. McNamara, and J. H. Bradford (2008), Comparison of instantaneous and constant-rate stream tracer experiments through non-parametric analysis of residence time distributions, *Water Resour. Res.*, *44*, W06404, doi:10.1029/2007WR006274.

Payn, R. A., M. N. Gooseff, B. L. McGlynn, K. E. Bencala, and S. M. Wondzell (2009), Channel water balance and exchange with subsurface flow along a mountain headwater stream in Montana, United States, *Water Resour. Res.*, *45*, W11427, doi:10.1029/2008WR007644.

Payn, R. A., M. N. Gooseff, B. L. McGlynn, K. E. Bencala, and S. M. Wondzell (2012), Exploring changes in the spatial distribution of stream baseflow generation during a seasonal recession, *Water Resour. Res.*, *48*, W04519, doi:10.1029/2011WR011552.

Poole, G. C. (2002), Fluvial landscape ecology: Addressing uniqueness within the river discontinuum, *Freshwater Biol.*, *47*, 641–660.

Runkel, R. L., D. M. McKnight, and E. D. Andrews (1998), Analysis of transient storage subject to unsteady flow: Diel flow variation in an Antarctic stream, *J. North Am. Benthol. Soc.*, *17*(2), 143–154.

Schmid, B. H. (2003), Temporal moments routing in streams and rivers with transient storage, *Adv. Water Resour.*, *26*(9), 1021–1027.

Shibata, H., O. Sugawara, H. Toyoshima, S. M. Wondzell, F. Nakamura, T. Kasahara, F. J. Swanson, and K. Sasa (2004), Nitrogen dynamics in the hyporheic zone of a forested stream during a small storm, Hokkaido, Japan, *Biogeochemistry*, *69*, 83–104.

Sivapalan, M. (2003), Process complexity at hillslope scale, process simplicity at the watershed scale: Is there a connection?, *Hydrol. Processes*, *17*, 1037–1041.

Stanford, J. A., and J. V. Ward (1993), An ecosystem perspective of alluvail rivers: Connectivity and the hyporheic corridor, *J. North Am. Benthol. Soc.*, *12*(1), 48–60.

Swanson, F. J., and M. E. James (1975), Geology and geomorphology of the H.J. Andrews Experimental Forest, Western Cascades, Oregon, Res. Pap. PNW-188, Pac. Northwest For. and Range Exp. Stn., For. Serv., U.S. Dep. of Agric., Portland, Oreg.

Triska, F. J., et al. (1990), In situ retention-transport response to nitrate loading and storm discharge in a third-order stream, *J. North Am. Benthol. Soc.*, *9*(3), 229–239.

Vervier, P., J. Gibert, P. Marmonier, and M. J. Dole-Oliver (1992), A perspective on the permeability of the surface freshwater-groundwater ecotone, *J. N. Am. Benthol. Soc.*, *11*(1), 93–102.

Voltz, T. J., M. N. Gooseff, A. S. Ward, K. Singha, M. Fitzgerald, and T. Wagener (2013), Riparian hydraulic gradient and stream-groundwater exchange dynamics in steep headwater valleys, *J. Geophys. Res. Earth Surf.*, *118*, 953–969, doi:10.1002/jgrf.20074.

Wagener, T., M. Sivapalan, P. Troch, and R. Woods (2007), Catchment classification and hydrologic similarity, *Geogr. Compass*, *1*(4), 901–931.

Wagner, B., and J. W. Harvey (1997), Experimental design for estimating parameters of rate-limited mass transfer: Analysis of stream tracer studies, *Water Resour. Res.*, *33*(7), 1731–1741.

Ward, A. S., M. N. Gooseff, and P. A. Johnson (2011), How can subsurface modifications to hydraulic conductivity be designed as stream restoration structures? Analysis of Vaux's conceptual models to enhance hyporheic exchange, *Water Resour. Res.*, *47*, W08512, doi:10.1029/2010WR010028.

Ward, A. S., M. N. Gooseff, M. Fitzgerald, T. J. Voltz, A. M. Binley, and K. Singha (2012), Hydrologic and geomorphic controls on hyporheic exchange during base flow recession in a headwater mountain stream, *Water Resour. Res.*, *48*, W04513, doi:10.1029/2011WR011461.

Ward, A. S., M. N. Gooseff, and K. Singha, (2013a), How does subsurface characterization affect simulations of hyporheic exchange? Ground Water, *51*, *14–28*.

Ward, A. S., R. A. Payn, M. N. Gooseff, B. L. McGlynn, K. E. Bencala, C. A. Kelleher, S. M. Wondzell, and T. Wagener (2013b), Variations in surface water-ground water interactions along a headwater mountain stream: Comparisons between transient storage and water balance analyses, *Water Resour. Res.*, *49*, 3359–3374, doi:10.1002/wrcr.20148.

White, D. S. (1993), Perspectives on defining and delineating hyporheic zones, *J. North Am. Benthol. Soc.*, *12*(1), 61–69.

Woessner, W. W. (2000), Stream and fluvial plain ground-water interactions: Re-scaling hydrogeologic thought, *Ground Water*, *38*(3), 423–429.

Wondzell, S. (2006), Effect of morphology and discharge on hyporheic exchange flows in two small streams in the Cascade Mountains of Oregon, USA, *Hydrol. Processes*, *20*(2), 267–287.

Wondzell, S. M., and F. J. Swanson (1996), Seasonal and storm dynamics of the hyporheic zone of a 4th-order mountain stream. I: Hydrologic processes, *J. North Am. Benthol. Soc.*, *15*(1), 3–19.

Wondzell, S. M., M. N. Gooseff, and B. L. McGlynn (2007), Flow velocity and the hydrologic behavior of streams during baseflow, *Geophys. Res. Lett.*, *34*, L24404, doi:10.1029/2007GL031256.

Wondzell, S. M., J. LaNier, and R. Haggerty (2009), Evaluation of alternative groundwater flow models for simulating hyporheic exchange in a small mountain stream, *J. Hydrol.*, *364*(1–2), 142–151.

Wondzell, S. M., M. N. Gooseff, and B. L. McGlynn (2010), An analysis of alternative conceptual models relating hyporheic exchange flow to diel fluctuations in discharge during baseflow recession, *Hydrol. Processes*, *24*, 686–694.

Zarnetske, J. P., M. N. Gooseff, W. B. Bowden, T. R. Brosten, J. H. Bradford, and J. P. McNamara (2007), Transient storage as a function of geomorphology, discharge, and permafrost active layer conditions in Arctic tundra streams, *Water Resour. Res.*, *43*, W07410, doi:10.1029/2005WR004816.

Zarnetske, J. P., R. Haggerty, S. M. Wondzell, and M. A. Baker (2011), Dynamics of nitrate production and removal as a function of residence time in the hyporheic zone, *J. Geophys. Res.*, *116*, G01025, doi:10.1029/2010JG001356.

Zarnetske, J. P., R. Haggerty, S. M. Wondzell, V. Bokil, and R. González-Pinzón (2012), Coupled transport and reaction kinetics control the nitrate source-sink function of hyporheic zones, *Water Resour. Res.*, *48*, W11508, doi:10.1029/2012WR011894.

Zellweger, G. W., R. J. Avanzino, and K. E. Bencala (1989), Comparison of tracer-dilution and current-meter discharge measurements in a small gravel-bed stream, Little Lost Man Creek, California, Water Resour. Invest. Rep., 89-4150, U.S. Geol. Surv., Denver, Colo.